10. TELESEISMIC OBSERVATIONS FROM OSS IV[1]

Rhett Butler and Frederick K. Duennebier, Hawaii Institute of Geophysics[2]

ABSTRACT

One of the primary objectives in placing seismic systems in deep-ocean boreholes is the detection of teleseismic earthquakes and nuclear events. If the oceanic basement is substantially quieter than the ocean floor and island sites, then the added data could yield information of considerable value in nuclear test detection. This chapter presents and evaluates data relevant to this problem.

The smallest teleseismic ($\Delta > 30°$) earthquake observed on the Hawaii Institute of Geophysics ocean sub-bottom seismometer (OSS) had a body-wave magnitude of 5.4. Only one nuclear explosion (m_b = 5.6) was clearly observed. With additional filtering and processing, nuclear explosions as small as m_b = 5.1 can be marginally observed. OSS records many regional earthquakes of the northwest circum-Pacific area that are not listed in the National Earthquake Information Service (NEIS) catalog. Teleseismic P-wave arrivals for several events contain frequencies as high as 8 Hz above the background noise. No teleseismic short-period S waves were seen, although high-frequency S waves from regional events were abundant. This dichotomy in the observability of S waves by OSS suggests that the lithosphere of the northwest Pacific has a high Q, but that the underlying asthenosphere is more highly attenuative.

INTRODUCTION

A deep-ocean marine borehole seismic system, the Hawaii Institute of Geophyics ocean sub-bottom seismometer (OSS), was successfully emplaced on 11 September 1982. The OSS is at the bottom of Hole 581C (43.924°N, 159.797°E), which was drilled through 357.6 m of sediment and 20.6 m of basalt in 5467 m of water by *Glomar Challenger* during Deep Sea Drilling Project (DSDP) Leg 88. The instrument detects seismic motion in three orthogonal directions (as well as two axes of tilt, and temperature). Data are multiplexed and digitized in the hole and passed up a wire either to a ship or to a recording package resting on the ocean floor (Duennebier and Blackinton, 1983; Byrne et al., this volume).

The OSS was designed and built at the Hawaii Institute of Geophysics in 1978 and emplaced twice in 1979 under funding from the National Science Foundation. Data from these experiments, the first on DSDP Leg 65 near the Tamayo Fracture Zone off Mexico and the second in the Guatemala Trench on Leg 67, are reported in Duennebier and Blackinton (1980) and Carter et al. (1984). These early experiments demonstrated the relative ease with which instruments can be permanently emplaced in deep-sea drill holes. A third experiment attempted on Leg 78A in 1981 failed because of a faulty design change in the tool.

After several design corrections and considerable testing, OSS IV was emplaced on 11 September 1982, in Hole 581C on DSDP Leg 88 with funding supplied by the Office of Naval Research. An array of 10 ocean-bottom seismometers was also emplaced around the drill site during the leg for a period of 2 weeks. The sole purpose of Leg 88, whose ship time was funded by the Defense Advance Research Projects Agency (DARPA), was to emplace a permanent borehole seismic system in a deep-sea drill hole. Drilling problems prevented emplacement of the Marine Seismic System (MSS), a DARPA-funded borehole seismic system that was later successfully emplaced on Leg 91. At the last minute, however, OSS IV was emplaced. It recorded more than 170 shots along four lines and a 5-km-radius circle fired by the *De Steiguer;* then, after the recorder package was lowered, it recorded continuous data for 64 days between 12 September and 16 November 1982. These data were recovered by the *Kana Keoki* on 12 May 1983; as the borehole instrument was operating perfectly, a second recording package was emplaced to record from 13 May to 14 July 1983.

The data recovered during the May 1983 reload are of excellent quality, from a large variety of identifiable sources. These include an average of about one regional earthquake per hour, several teleseismic events, and variations in noise level believed to be caused by the passage of storms, whales, and ship traffic. The recovery crew were extremely lucky to be on site and recording data in real time at 100 samples/s when the magnitude 7.8 Japan quake occurred at a distance of 16° (Duennebier, this volume). This quake, which was actually felt by people aboard the *Kana Keoki*, produced an unclipped record with signal well above noise over more than 11 octaves.

This chapter presents a preliminary analysis of observability of earthquakes and explosions on the OSS system. A large number of northwest circum-Pacific earthquakes were recorded by OSS, many of which are not located in the NEIS catalog. An effort is underway to coordinate location of many events in cooperation with our Russian colleagues, who operate seismic stations in Kamchatka and the Kuriles. However, the great number of events and lack of locations have overwhelmed our effort to place constraints on the regional observability of earthquakes on the OSS system. The only statement

[1] Duennebier, F. K., Stephen, R., Gettrust, J. F., et al., *Init. Repts. DSDP*, 88: Washington (U.S. Govt. Printing Office).

[2] Addresses: (Butler, Duennebier) Hawaii Institute of Geophyics, University of Hawaii at Manoa, Honolulu, HI 96822.

that can reliably be made until the signals are correlated with the Soviet data is that the OSS records many events in the northwest circum-Pacific that are not detected and located teleseismically on global seismic network stations (see Cessaro and Duennebier, this volume).

To place more quantitative constraints on event observability at OSS, a more restricted class of events was examined: teleseismic events at distances greater than 30°Δ (geocentric angle) from OSS. In this effort we attempt to determine the smallest event in terms of body-wave magnitude, m_b, that can be observed on the OSS system. The present results should be considered preliminary for two reasons: (1) all teleseismic events were not examined—only a subset of larger events was considered, and (2) only events occurring within the 12 September through 16 November 1982 recording period were available—additional data recorded between 12 May and 14 July 1983 by OSS have not yet been funded to be retrieved. Background noise level variation plays an important part in earthquake observability, and some instances of varying noise effects will be noted. The discussion of noise levels at OSS is deferred to a companion report (see Duennebier et al., this volume).

INSTRUMENT CHARACTERISTICS

A complete description of the OSS system can be found in this volume and in Duennebier and Blackinton (1983). The seismic sensors are HS-1 Geospace 5-kΩ coil, 4.5-Hz geophones. Nine geophones are placed in a vertical string and connected in series (each 50% damped) to supply vertical velocity, and two horizontal geophones are arranged in series to give horizontal velocity in orthogonal horizontal directions. The instrument is lowered to the bottom of the hole and clamped by pressing a pad (containing the vertical geophones) against the side of the hole. The tool is within 4° of vertical and has at least five points of hard contact with the walls and bottom of the hole. The sensitive azimuths of the horizontal geophones have been determined by measurement of the polarity and amplitudes of shots fired in a circle around the hole. One horizontal geophone detects motion within a few degrees of positive East, and the other positive South; the vertical is positive for upward velocity.

Data are sampled and digitized at a rate of 100 samples/s when recording is in real time and 50 samples/s when it is by the recording package. Data are floating point with an 8-bit mantissa, a sign bit, and a 3-bit (factor of 4) exponent for a dynamic range of 132 dB. Direct current (DC) offsets are removed from the data periodically and recorded separately. Data are sent up the cable in delay modulation format to be either (1) recorded on standard audio tape on a surface ship for later decoding, (2) decoded and converted to analog in a test box for strip chart recording, or (3) converted to analog and recorded continuously, together with time and gain information in gain-ranging analog format in the recording package. Although dynamic range is certainly lost in the recorder package by changing from digital back to analog, the net gain from having a long period of continuous information far exceeds the loss of dynamic range. Upon return to the Hawaii Institute of Geophysics, all data can be related back to true ground velocity within a few decibels. Timing accuracy on real-time data is to about 0.01 s, and accuracy for recorded data is believed to be about 0.2 s after correction for drift. The poor timing accuracy is because the recorders were picked up 6 months after the 2-month recording period.

OBSERVATIONAL METHODS

Two methods were used to determine the lower magnitude limit for observability of teleseismic events: one relatively simple, the other relatively sophisticated. In the first instance, the three-component raw digital data were plotted merely to see if a particular event is visible within a time window determined by the distance and depth of the event and the body-wave travel time calculated from the Jeffreys–Bullen (1958) seismological tables. If the event is visible at the appropriate time, then the primary criterion of observability is met. If the event is not visible, however, it does not mean that we have crossed the threshold of observability for the system. It may be that noise masks the signal, but that with suitable band-pass filtering a portion of the signal may be observable. Further, lack of observation of an earthquake at OSS may mean that the event has a source radiation node in the direction of OSS. Explosions with isotropic sources do not have radiation nodes and therefore represent a more reliable subset of data to examine.

To look for events visibly immersed in the background noise, we applied the quasi-harmonic decomposition (QHD) method of C. B. Archambeau et al. (pers. comm., 1984), which uses both time and frequency domain information to detect signals of a particular character. The following discussion of QHD is adapted from C. B. Archambeau et al. (pers. comm., 1984). Fundamentally, QHD analysis consists of parallel filtering of the time series with a set of gaussian narrow-band filters. The output of each filter corresponds to a single quasi-harmonic component of the original time series and has the form of a modulated sinusoid. The modulation of the sinusoidal output contains information concerning the time of energy arrivals within the time series, whereas the carrier sinusoid contains the spectral information related to the arrivals. Seismic body waves are undispersed transients, and therefore, group arrivals in different frequency bands arrive simultaneously. This characteristic may be used to distinguish a body wave from incoherent noise for which group arrival times in different frequency bands are poorly correlated. In a QHD of a time series, the envelope function of each narrow-band filter output is formed. The time and instantaneous amplitude of each envelope maximum (peak) are stored for each filter band. A computer-aided pattern recognition algorithm searches the time-frequency plane for peaks forming coherent ridges at a particular time across a band of frequencies. The time uncertainty window (Δt) is related to the filter bandwidth ($\Delta\omega$) by the uncertainty principle ($\Delta t \Delta\omega = 1/2$ for gaussian filters). For each detection made, the use of the instantaneous amplitude and the phase information associated with each peak allows reconstitution of the detection data into time-do-

main waveform. The amplitude and phase characteristics of the detection together with the traveltime form a basis for judgement as to whether a detection meets the criteria of a particular body-wave arrival.

OBSERVATIONS

Two classes of teleseismic ($\Delta > 30°$) sources were examined in OSS IV data: earthquakes and nuclear explosions. The largest earthquake occurring during the recorder package operational period (12 September through 16 November 1982) was a m_b = 6.2 deep-focus (d = 515 km) earthquake on 7 October in the Banda Sea. The largest explosion was a m_b = 5.6 event on 1 October in Novaya Zemlya. Compressional waves for both events were recorded on the OSS system.

Compressional and shear-wave energy from teleseismic events approaches OSS at relatively steep angles of incidence ($< 28°$). The direct, mantle-refracted ray interacts with sediment and water layers above OSS, and thus the wavefield recorded includes these local elastic effects. Figure 1 illustrates the primary rays generated by local structure from an incident compressional wave. The actual times and amplitudes of the rays depend upon the ray parameter of the incoming P wave.

The first reflection from the base of the sediments overlying OSS arrives about one-hundredth of a second after the direct P wave, with an amplitude about 50% in size and with the same polarity. The wave polarity exhibits a 180° phase shift at the interface, but since the vector direction of wave propagation has also reversed, no polarity reversal is observed on the vertical component. These two phases add constructively on the vertical component and destructively on the radial horizontal component. As the velocity is decreasing upward, most energy is transmitted upward. The S velocity in the basement is nearly equal to the P velocity in the sediment; thus there is a good impedance match between compressional waves in the basement and shear waves in the sediments. About half a second after the direct P wave, the reflection from the bottom of the ocean arrives with an amplitude about 30% of the direct P wave and with the same polarity. At about 7.9 s following the direct P waves, the reflection from the ocean surface arrives, again without polarity reversal. Sediment reverberations, P-to-S converted phases, and crustal interactions are also present. From this simple enumeration of wave-field interactions above OSS, we note that in viewing data from OSS, the convolution of the local structure with the incoming wavefield should not be neglected.

Figures 2, 3, and 4 plot the P-wave motion for each of three earthquakes: the m_b = 6.2 event in the Banda Sea mentioned at the beginning of this section, a m_b = 5.9 deep-focus earthquake south of Fiji, and a m_b = 5.4 intermediate depth earthquake east of the Celebes Sea. Three components (one vertical and two horizontal) of ground velocity are shown in each figure. The m_b = 5.4 earthquake is the smallest teleseismic event clearly observed on the OSS.

No short-period S waves were observed for any of these events. The lack of short-period S wave observations is surprising. Deep-focus earthquakes often yield better recordings of short-period S waves than shallow events. This is because of high attenuation in the upper mantle: S waves from deep-focus earthquakes are essentially attenuated only once in propagation from source to receiver, whereas S waves from shallow events are attenuated twice. It is very unlikely that OSS IV lies on a radiation null for all of the earthquakes examined, especially since SH and SV do not in general share radiation nulls. The lack of observable S waves at OSS suggests that attenuation beneath the northwestern Pacific litho-

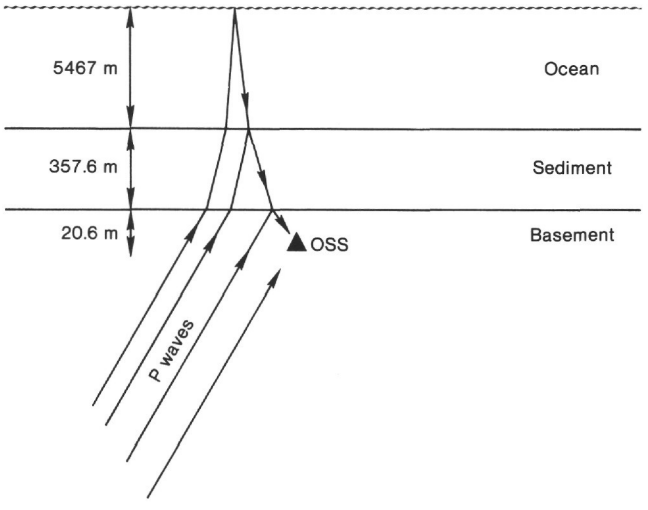

Figure 1. Teleseismic P waves recorded by OSS interact with sediment and water layers above the instrument. Illustrated are the direct P wave and primary reflections from the sediment/bedrock and sediment/water interfaces as well as from the ocean surface. Layer thicknesses are indicated in the figure, which is not drawn to scale.

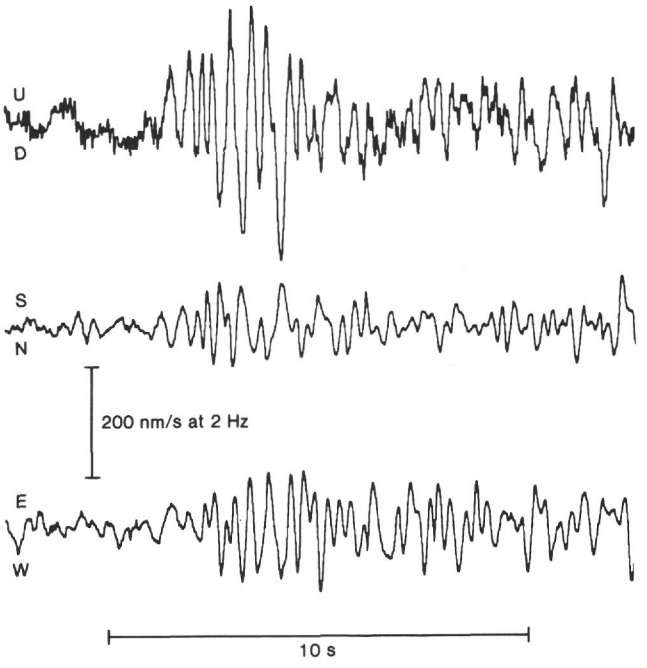

Figure 2. Vertical and horizontal components of velocity recorded by OSS IV are shown for the P wave from a m_b = 6.2 earthquake in the Banda Sea: origin time 7 October 1982, 7:15:56.6; epicentral location 7.156°S, 125.876°E; depth 515 km; Δ = 59.5°. The velocity scale is in nanometers per second.

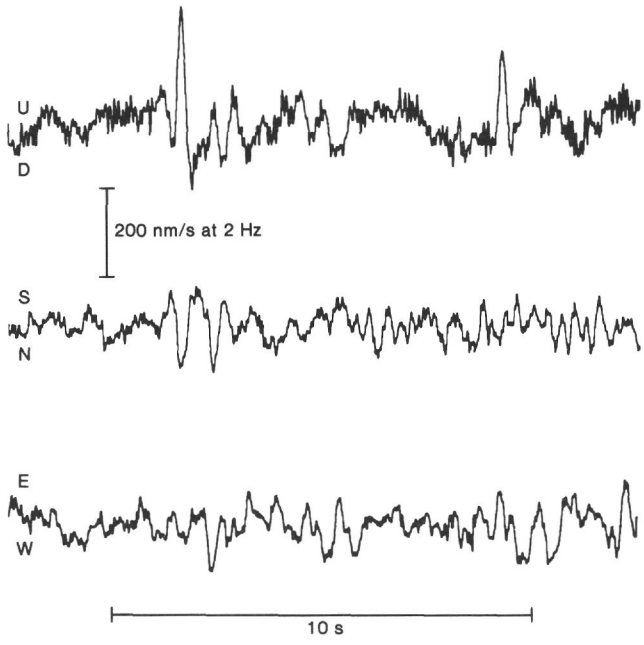

Figure 3. Vertical and horizontal components of velocity recorded by OSS IV are shown for the P wave from a m_b = 5.9 earthquake south of Fiji: origin time 17 September 1982, 13:28:24.8; epicentral location 23.469°S, 179.852°W; depth 546 km; Δ = 69°. The velocity scale is in nanometers per second.

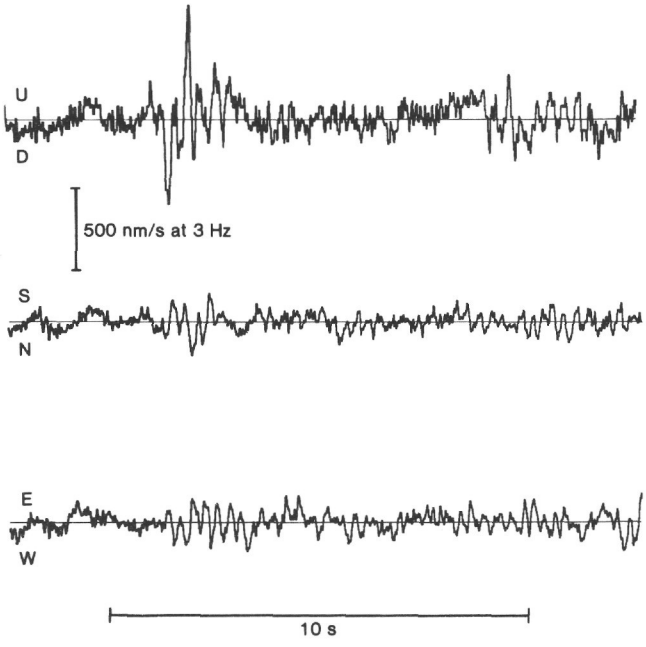

Figure 4. Vertical and horizontal components of velocity recorded by OSS IV are shown for the P wave from a m_b = 5.4 earthquake east of the Celebes Sea: origin time 8 November 1982, 18:35:34.7; epicentral location 4.827°N, 127.860°E; depth 160 km; Δ = 48.1°. The velocity scale is in nanometers per second.

sphere is probably severe. Regional events, however, yielded abundant high-frequency Sn recordings at OSS, indicating that the lithosphere itself has a relatively high Q.

Figure 5 displays three components of the P-wave motion recorded for the m_b = 5.6 Novaya Zemlya nuclear

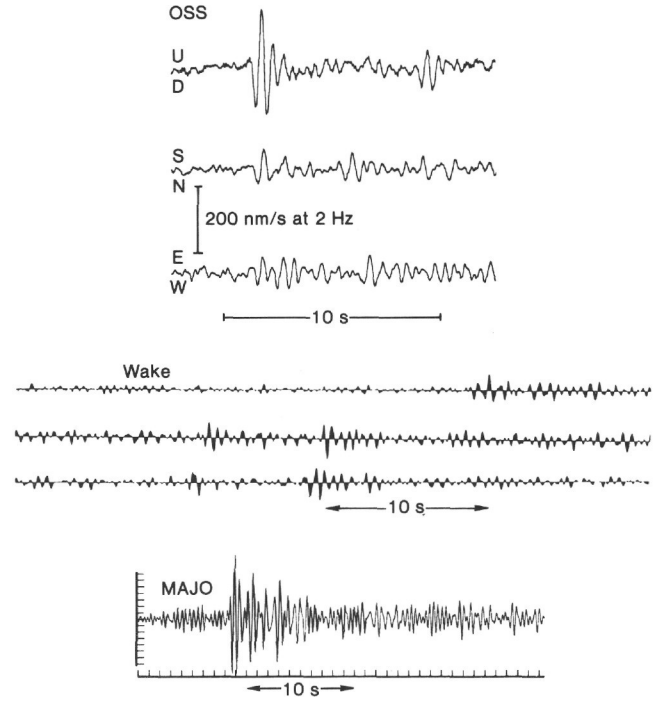

Figure 5. Signal quality at three seismic station sites is compared for the same event. The upper traces are vertical and horizontal components of velocity recorded by OSS IV for the P wave from a m_b = 5.6 Russian nuclear explosion in Novaya Zemlya: origin time 11 October 1982, 7:14:58.2; epicentral location 73.392°N, 54.559°E; Δ = 52.5°). The velocity scale is in nanometers per second. In the middle of the figure data from the Wake Hydrophone Array are displayed. The lower two traces from Wake are bottom hydrophones separated by less than 20 km, whereas the upper trace is a recording from a more distant hydrophone suspended in the SOFAR channel. The hydrophones record pressure. The bottom trace is from the short-period vertical component of the SRO station MAJO in Japan and it displays ground displacement.

explosion on 1 October 1982, together with arrivals from the Wake Island bottom hydrophone array and station MAJO in Japan. This is the largest explosion that occurred during the operational period of the OSS recording package. The signal-to-noise ratio on the OSS is at least a factor of two better than on the other two stations. During the recording period a total of 15 nuclear explosions were reported to the Center for Seismic Studies in Arlington, VA. Waveform similarities among nuclear explosions make these sources ideal for judging observability. Unlike earthquake waveforms, which vary considerably between events, nuclear explosions have a predictable waveform. Of the 15 explosions reported during the OSS recording period, only the largest event (shown in Fig. 5) was clearly visible. The primary reason that the other large events were not observed was that the background noise below 3 Hz had increased. Because the m_b = 5.6 event contained frequencies as high as 6.5 Hz, the observation window for the other nuclear events was shifted to higher frequency to take advantage of the high-frequency character of the source and the lower noise environment.

QHD analysis was performed on the largest event and 10 of the 14 nuclear events not observed in the simple

play out of the recordings. The largest event served as a template in matching the waveform character of the other events, and the Jeffreys–Bullen traveltime served as parallel sieve in windowing the detections. Following this procedure, 3 out of the 10 events examined yielded arrivals at the appropriate time and with waveshapes similar to the largest clearly recorded explosion, although distorted by the noise. The magnitudes and dates of these events are: (1) m_b = 5.2 on 21 September, (2) m_b = 5.1 on 25 September, and (3) m_b = 5.3 on 10 October. Although these events are only marginally observable with sophisticated processing, their detection suggests that under restricted circumstances the minimum magnitude observable by the OSS is about m_b = 5.1 for high-frequency events. This level of observability is not uniform but depends upon the daily variation of background noise.

Magnitude detection thresholds reported in the literature for other sites cannot be compared in a straightforward manner with the results present herein, but their mention is useful. In the distance range 30° to 90°Δ, Dahlman and Israelson (1977) reported m_b detection thresholds of 3.8–4.0 for the Large Aperture Seismic Array (LASA), 4.2 for the Norwegian Seismic Array (NORSAR), and 4.5 for the Yellowknife array. These values are for large seismic arrays composed of many sensors. For 32 individual seismic stations distributed worldwide, Dahlman and Israelson reported detection thresholds at or below m_b = 5.0 for 80% of the stations; the highest threshold value was m_b = 5.3. These values for individual stations are, however, influenced by events at local and regional (<30°) distances not included in the present, preliminary analysis of the OSS data. It is clear that the OSS is highly sensitive to local and regional events with small m_b. In a study of Russian nuclear explosions recorded on short-period (1-s) World Wide Standard Seismograph Network (WWSSN) stations in the United States (Butler, 1984), the smallest event that could be clearly observed at more than half of the 25 available stations had a m_b = 5.7, with smaller events observable at only a few stations.

FREQUENCY CONTENT OF SIGNALS

QHD analysis was applied to each event observed to determine where the signal drops into the high-frequency noise. The QHD frequency–time (f-t) plane presents a clear illustration of the frequency content of the signals. Figures 6 and 7 show the f-t planes for two events: the m_b = 5.6 nuclear explosion from Figure 5 is shown in Figure 6 and the m_b = 5.4 intermediate (160 km) depth earthquake of Figure 4 is shown in Figure 7.

A 25.6-s (2048 sample) window containing the observed P wave (vertical component of velocity) is plotted above the f-t plane in each figure. Below the time series are plotted the locations in frequency and time of amplitude peaks from the gaussian narrow-band filters. These amplitude peaks are local maxima in the envelope function of each filter band. Filter bands are arranged by row from lower to higher frequency. Amplitude peaks at corresponding times are represented symbolically: the largest peak in each band by "*" and other peaks as a number scaled as tenth of the maximum. Thus, a "2" represents a peak that is about 20% of the maximum peak "*". Each band is scaled independently.

Beneath the P-wave arrivals shown in Figures 6 and 7, note the coherent vertical ridge formed by the maximum amplitude "*" arrivals in each filter band aligning at nearly the same time. The time uncertainty of the filter bands used is 0.1 s, and the effective bandwidth of the filters is approximately ±1.5 Hz.

The representation of the QHD f-t plane allows us to observe clearly the temporal relationships and frequency contents of signal pulses, as well as the signal-to-noise relationship in each filter band. For the nuclear explosion in Figure 6, frequencies as high as 6.5 Hz are above the noise level preceding the signal. Above 6.5 Hz the signal rapidly fades into the noise. For the intermediate depth earthquake in Figure 7, the frequency content of the P wave extends to 8 Hz before dropping into the noise (higher frequency filter bands are not shown). Frequencies as high as 8 Hz and 4.5 Hz, respectively, were found in the P waves of the m_b = 6.2 earthquake of Figure 2 and the m_b = 5.9 earthquake in Figure 3. Frequencies as high as 9 Hz have been observed at the Wake Island hydrophone array from teleseismic events (McCreery et al., 1983). Correspondingly high frequencies have been observed on land at the LASA in Montana and reported by Evernden (1977) and Evernden and Kohler (1979). Frequencies as high as 10 Hz have been observed at NORSAR from a Russian nuclear explosion (Trourud, 1983).

CONCLUSIONS

The OSS IV seismometer records teleseismic P waves from earthquakes and explosions with a performance as good as that of most land-based instruments. The frequency contents of teleseismic P waves observed are rich in high frequencies (up to 8 Hz). The smallest teleseismic event clearly observed had a m_b = 5.4. No teleseismic short-period S waves were observed, although S waves from regional earthquakes were observed. The lack of teleseismic S waves coupled with observations of high-frequency Sn from regional earthquakes suggests that the lithosphere of the northwest Pacific has a high Q whereas the underlying asthenosphere or upper mantle must have a relatively low Q for S waves.

ACKNOWLEDGMENTS

This report has been critically reviewed by G. Sutton, C. S. McCreery, and R. K. Cessaro. Funding for this analysis was supplied by the Office of Naval Research and the Hawaii Institute of Geophysics. This is Hawaii Institute of Geophysics Contribution No. 1669.

REFERENCES

Butler, R., 1984. Azimuth energy, Q, and temperature: variations on P-wave amplitudes in the United States. *Rev. Geophys. Space Phys.*, 22:1–36.

Carter, J. A., Duennebier, F. K., and Hussong, D. M., 1984. A comparison between a downhole seismometer and a seismometer on the ocean floor. *Bull. Seismol. Soc. Am.*, 74:763–772.

Dahlman, O., and Israelson, H., 1977. *Monitoring Underground Nuclear Explosion:* New York (Elsevier).

Duennebier, F. K., and Blackinton, G., 1980. A man-made hot spring on the ocean floor. *Nature*, 284: 338.

_____, 1983. The ocean sub-bottom seismometer. *In* Geyer, R. A. (Ed.), *CRC Handbook of Geophysical Exploration at Sea*: Boca Raton, Florida (CRC Press), pp. 317–332.

Evernden, J., 1977. Spectral characteristics of the P codas of Eurasian earthquakes and explosions. *Bull. Seism. Soc. Am.*, 67:1153–1172.

Evernden, J., and Kohler, W., 1979. Further study of the spectral characteristics of P codas of earthquakes and explosions. *Bull. Seism. Soc. Am.*, 69:483–511.

Jeffreys, H., and Bullen, K. E., 1958. *Seismological Tables:* London (Brit. Assoc. Adv. Sci., Gray-Milne Trust).

McCreery, C. S., Walker, D. A., and Sutton, G. H., 1983. Spectra of nuclear explosions, earthquakes, and noise from Wake Island bottom hydrophones. *Geophys. Res. Lett.*, 10:59–62.

Trourud, L., 1983. Scientific Report 1-82/83, Norwegian Seismic Array (NORSAR), Kjeller, Norway.

Date of Initial Receipt: 11 June 1984
Date of Acceptance: 23 September 1985

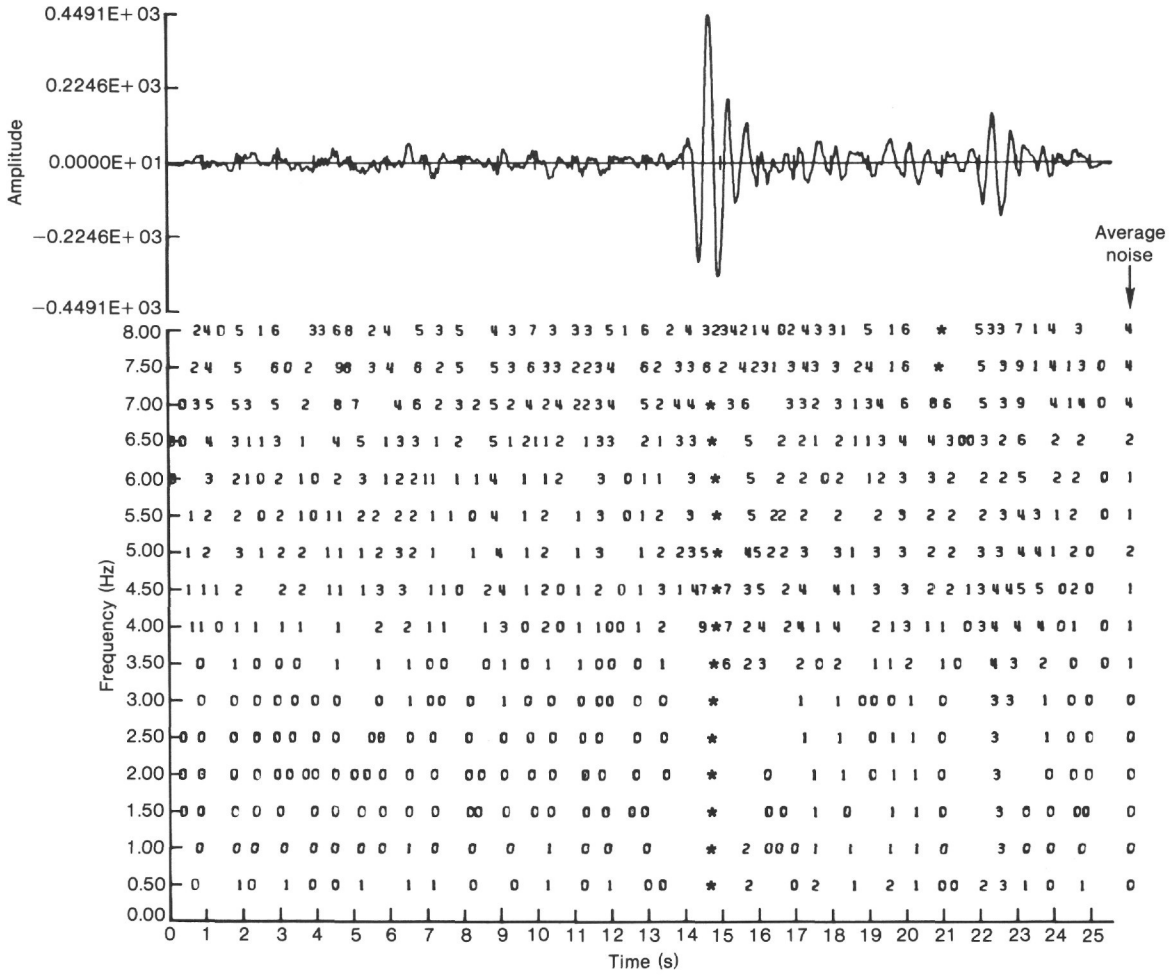

Figure 6. The upper trace plots the vertical component of velocity as recorded by OSS IV for the P wave from the nuclear explosion in Figure 5. Below the trace is the QHD time-frequency plane. Each row of numbers represents a gaussian filter band. The numbers indicate the amplitudes of local maxima in the envelope function of each band, and their position gives the time and frequency. The largest value in each filter band is marked by a "*", other peaks are numbers representing tenths of this maximum, that is, "2" is 20 to 29% of the maximum. Average noise levels in each band are shown by the farthest number to the right. Note the coherent vertical ridge of maximum amplitude values (*) beneath the P wave.

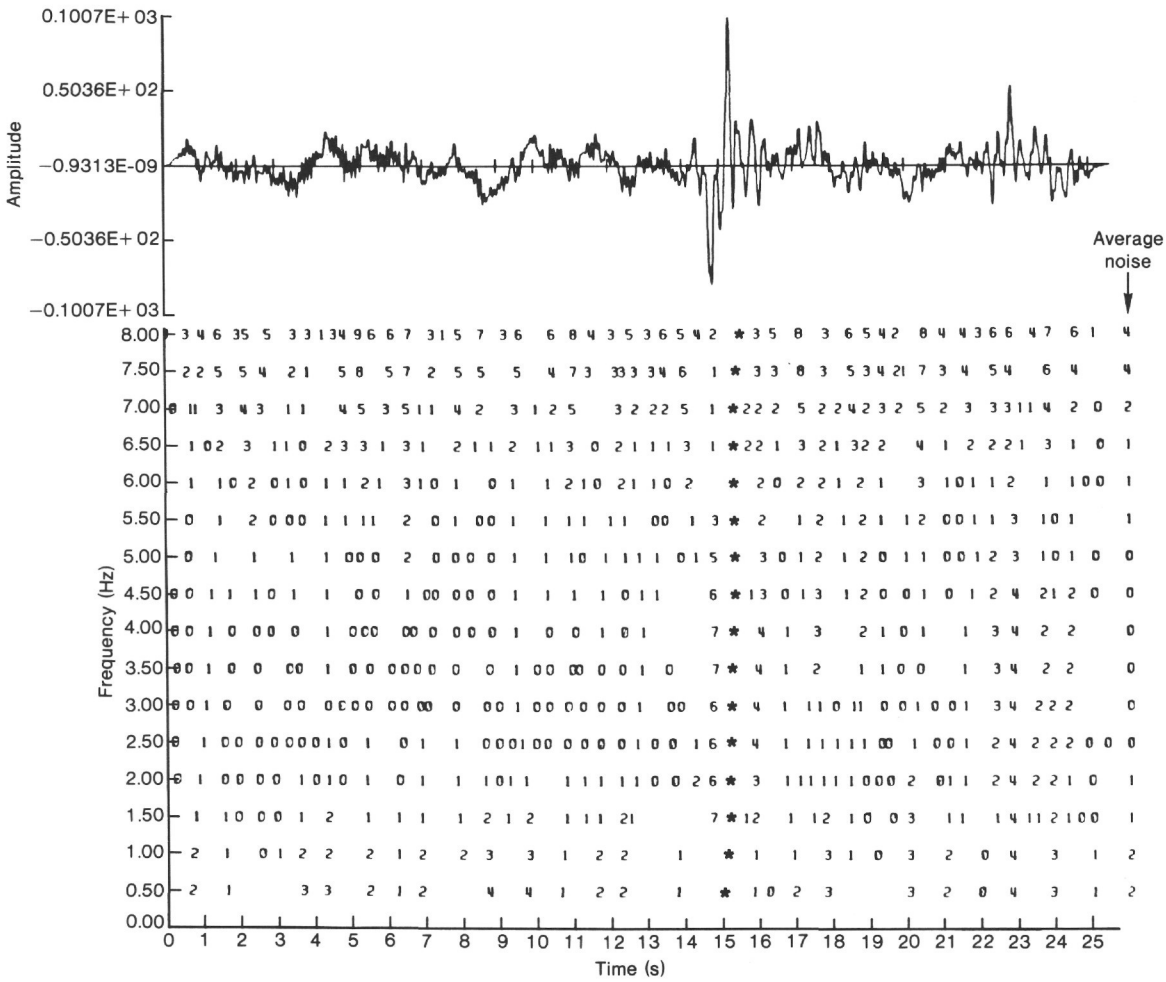

Figure 7. The upper trace plots the vertical component of velocity as recorded by OSS IV for the P wave from the earthquake in Figure 4. See Figure 6 for an explanation of the figure. Note the coherent vertical ridge of maximum amplitude values (*) beneath the P wave.